Supporting Information

Metallic BSi_3 Silicene: A Promising High Capacity Anode Material for Lithium-Ion Batteries

Xin Tan, Carlos R. Cabrera, Zhongfang Chen[*]

Department of Chemistry, Institute for Functional Nanomaterials, University of Puerto Rico, Rio Piedras Campus, San Juan 00931, Puerto Rico

[*] Corresponding author: zhongfangchen@gmail.com (Z.C.)

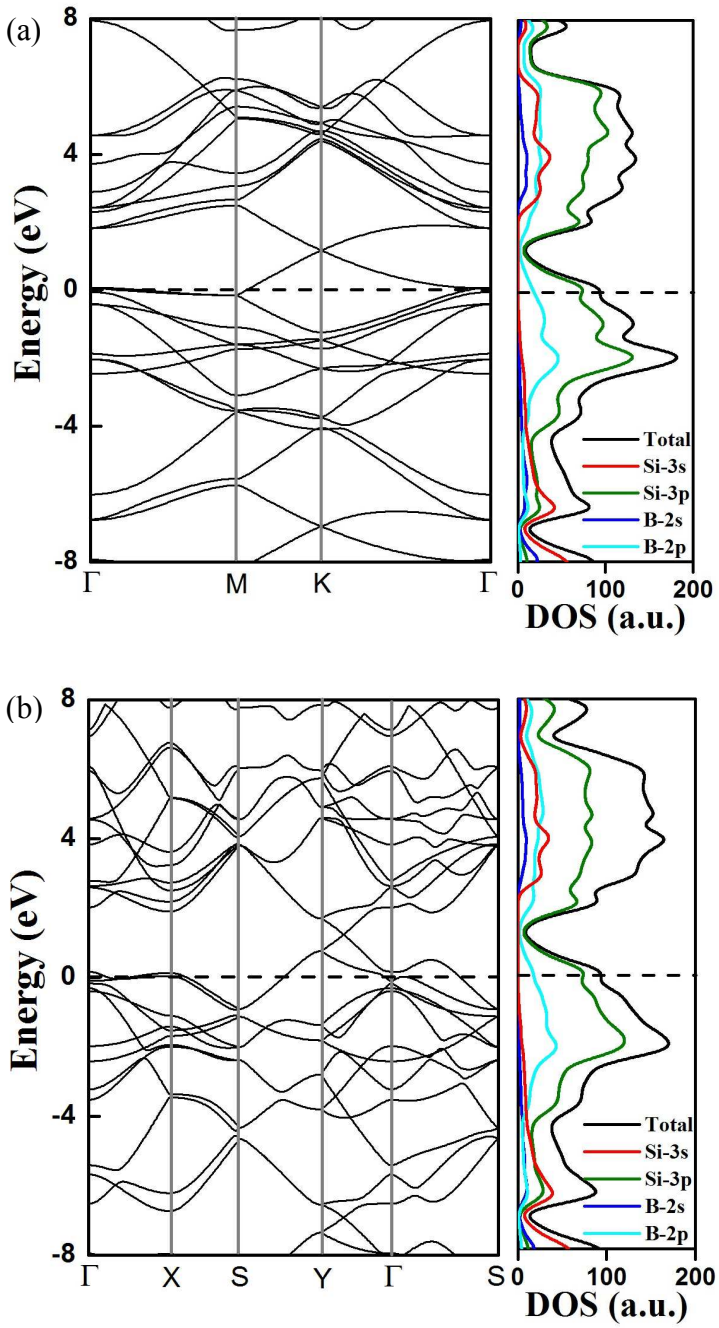

Figure S1. Calculated electronic band structure (left) and density of states (DOS, right) of the SL (a) *H*-BSi_3 and (b) *R*-BSi_3. The DOS is projected on Si-3s, Si-3p, B-2s, B-2p.

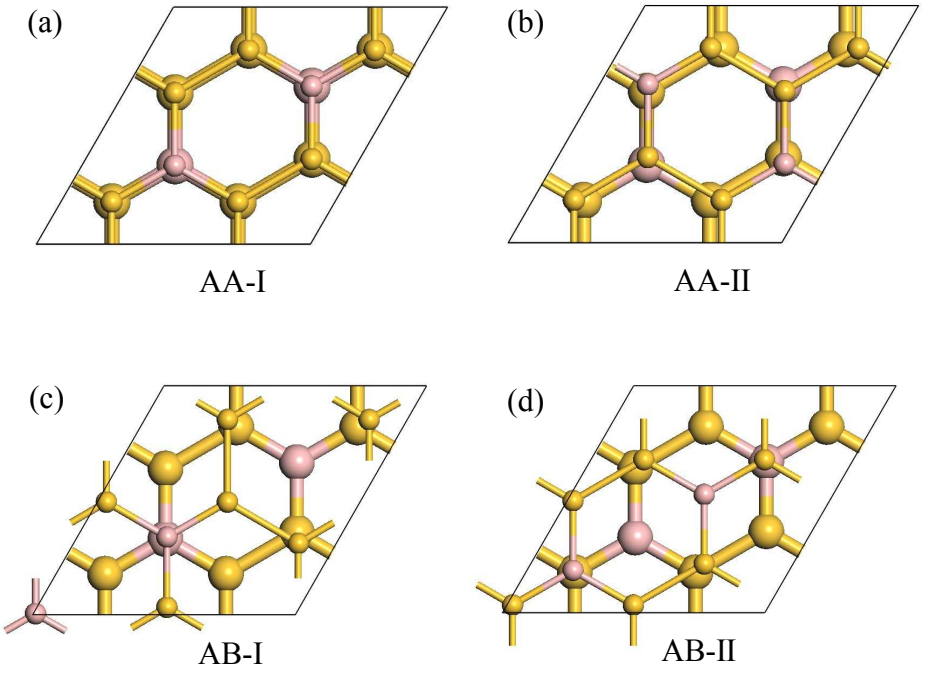

Figure S2. The possible atomic arrangements of *H*-BSi_3 with (a)-(b) AA and (c)-(d) AB stacking. The yellow and light magenta spheres denote Si and B atoms, the Si/B atoms in the bottom layer and upper layer are represented by large and small spheres, respectively.

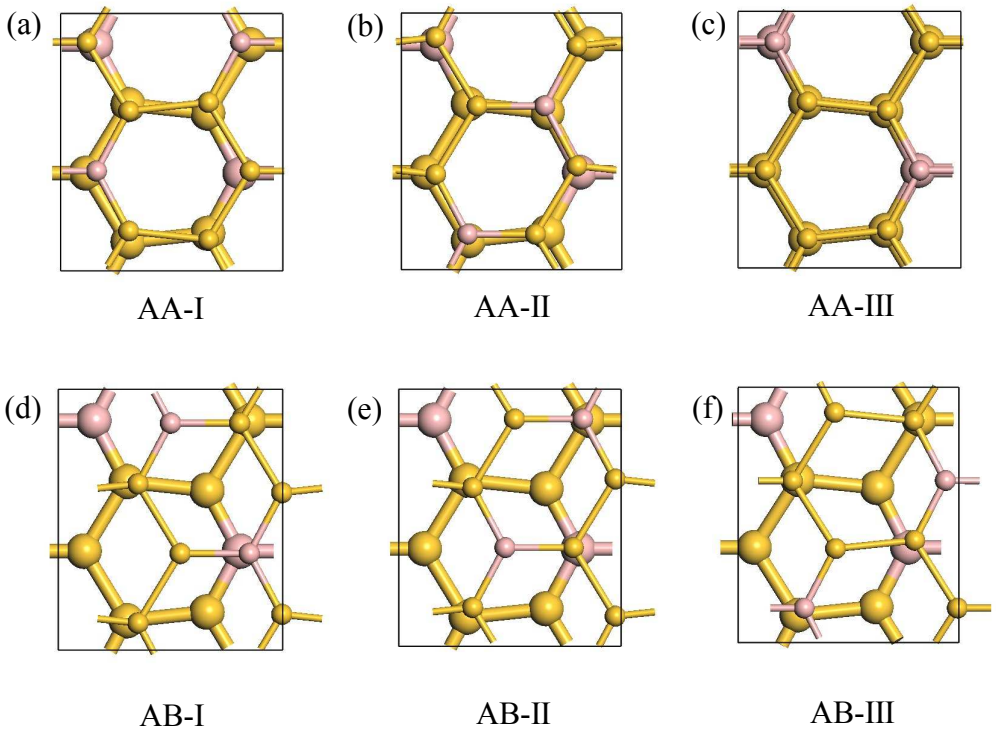

Figure S3. The possible atomic arrangements of *R*-BSi_3 with (a)-(c) AA and (d)-(f) AB stacking. The yellow and light magenta spheres denote Si and B atoms, the Si/B atoms in the bottom layer and upper layer are represented by large and small spheres, respectively.

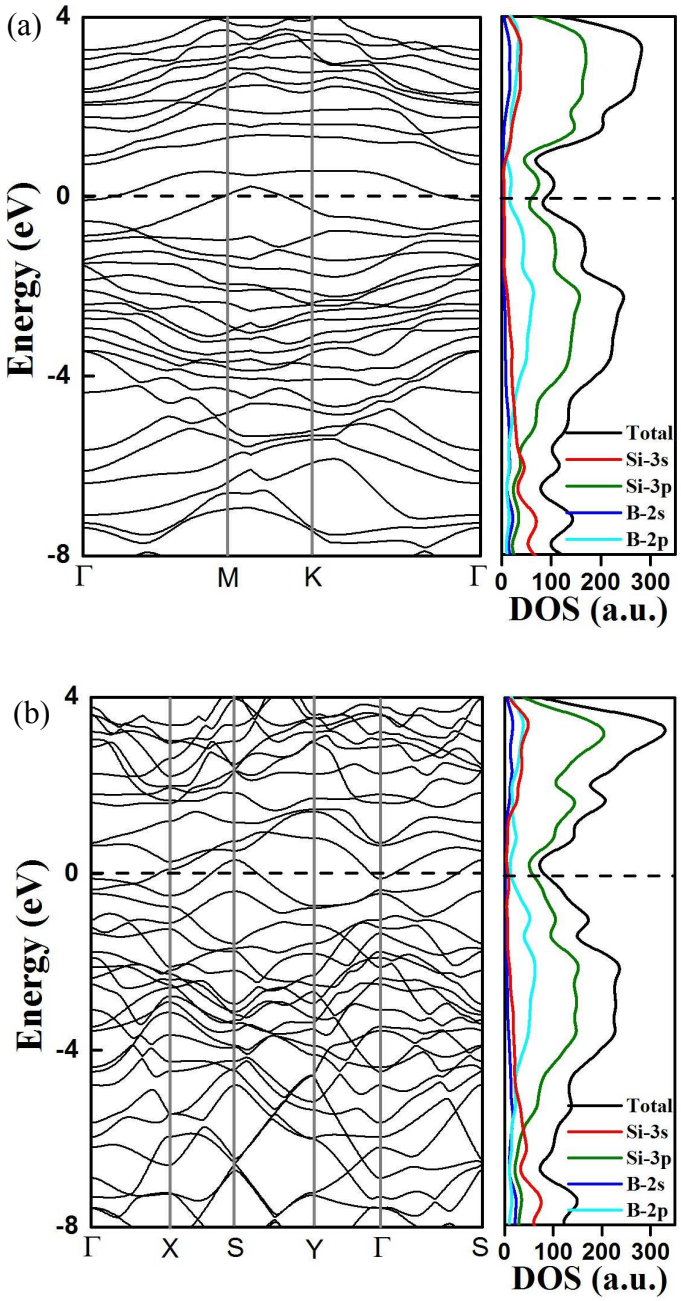

Figure S4: Calculated electronic band structure (left) and density of states (DOS, right) of the DL (a) *H*-BSi_3 and (b) *R*-BSi_3. The DOS is projected on Si-3s, Si-3p, B-2s, B-2p.

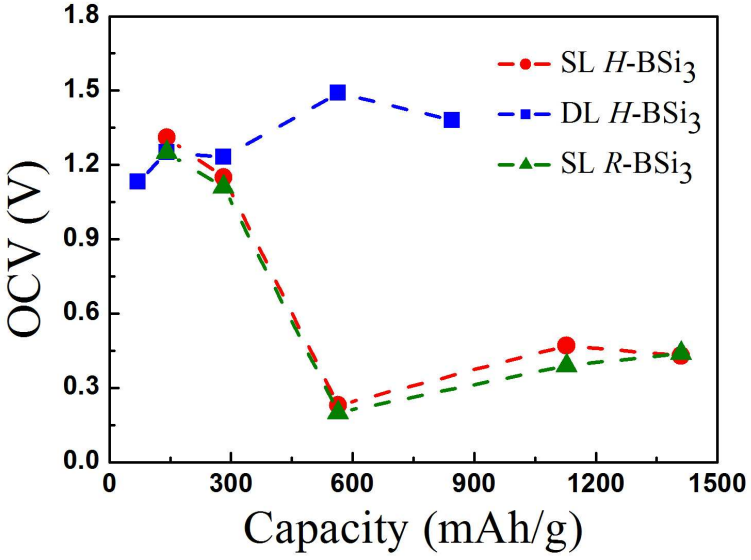

Figure S5: OCV as a function of charge capacity of SL *H*-BSi_3 (red), DL *H*-BSi_3 (blue), and SL *R*-BSi_3 (green).

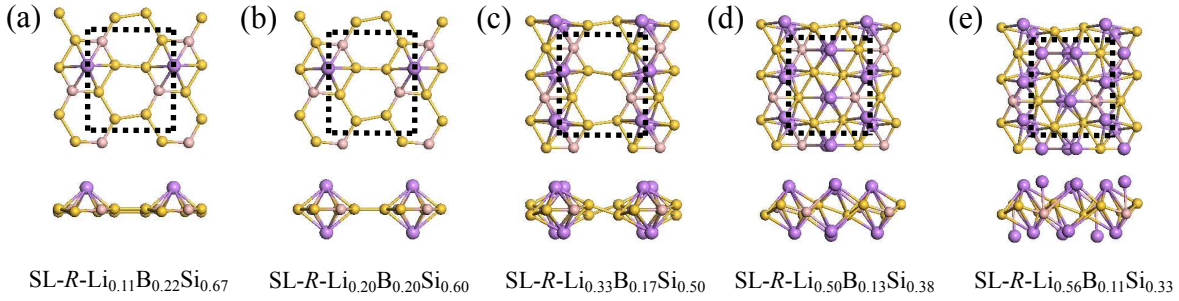

Figure S6. (a)-(e) The lowest-energy structures of lithiated SL *R*-BSi_3, SL-*R*-$Li_xB_{0.25(1-x)}Si_{0.75(1-x)}$ with different Li content *x*. Top (upper) and side (lower) views are shown separately, and the unit cell is denoted in each top view.

The same as SL *H*-BSi_3, for SL *R*-BSi_3, when the unit cell contains only a single Li atom (SL-*R*-$Li_{0.11}B_{0.22}Si_{0.67}$), the Li atom adsorbs preferably at H_2 site (Figure S5a), where the Li resides above the center of the hexagonal ring consisting of six Si and two B atoms. The corresponding adsorption energy (2.96 eV) at H_2 site is 0.01 and 0.33 eV higher than that at H_1 and T_B sites, respectively.

Up to 10 Li atoms can be can favorably adsorbed in each unit cell of SL *R*-BSi_3 (Figure S5b-e), which is the same as the case of the SL *H*-BSi_3. When only two Li atoms are adsorbed in a unit cell, i.e., for SL-*R*-$Li_{0.20}B_{0.20}Si_{0.60}$ (Figure S5b), these two Li are reside above and below a single H_2 site with E_{ads}=2.89 eV and OCV=1.11 V. As Li content increases, taking SL-*R*-$Li_{0.50}B_{0.13}Si_{0.38}$ (Figure S5d) as an example, eight Li gradually cover the two SL r-BSi_3 surfaces with the adsorption energy and OCVs are 2.25 eV and 0.39 V, respectively. At high Li content (SL-*R*-$Li_{0.56}B_{0.11}Si_{0.33}$) (Figure S5e), five Li (four at the hollow sites and one at T_B site) are above and five Li are below (four at the hollow sites and one at T_B site) the *R*-BSi_3 monolayer, and the

corresponding adsorption energy and OCVs are 2.23 eV and 0.44 V, respectively.

When further increasing the Li content (x>0.56), the Li adsorption energy and OCV decrease significantly. For instance, at the Li content of x=0.6, the adsorption energy and OCV are 2.04 eV and -0.62 V, respectively. Thus, we used SL-*R*-$Li_{0.56}B_{0.11}Si_{0.33}$ to represent the fully lithiated structure of SL *R*-BSi_3.

The charge capacity of the SL *R*-BSi_3 (1410 mA·h/g) is the same as that of the SL *H*-BSi_3. Additionally, the average Li adsorption energy decreases with increasing the lithiation ratio, from 2.96 for x=0.11 to 2.23 eV for x=0.56 (Figure 3f), and the OCV decrease from 1.25 to 0.44 V (Figure 3g), which are quite similar to the case of SL *H*-BSi_3.

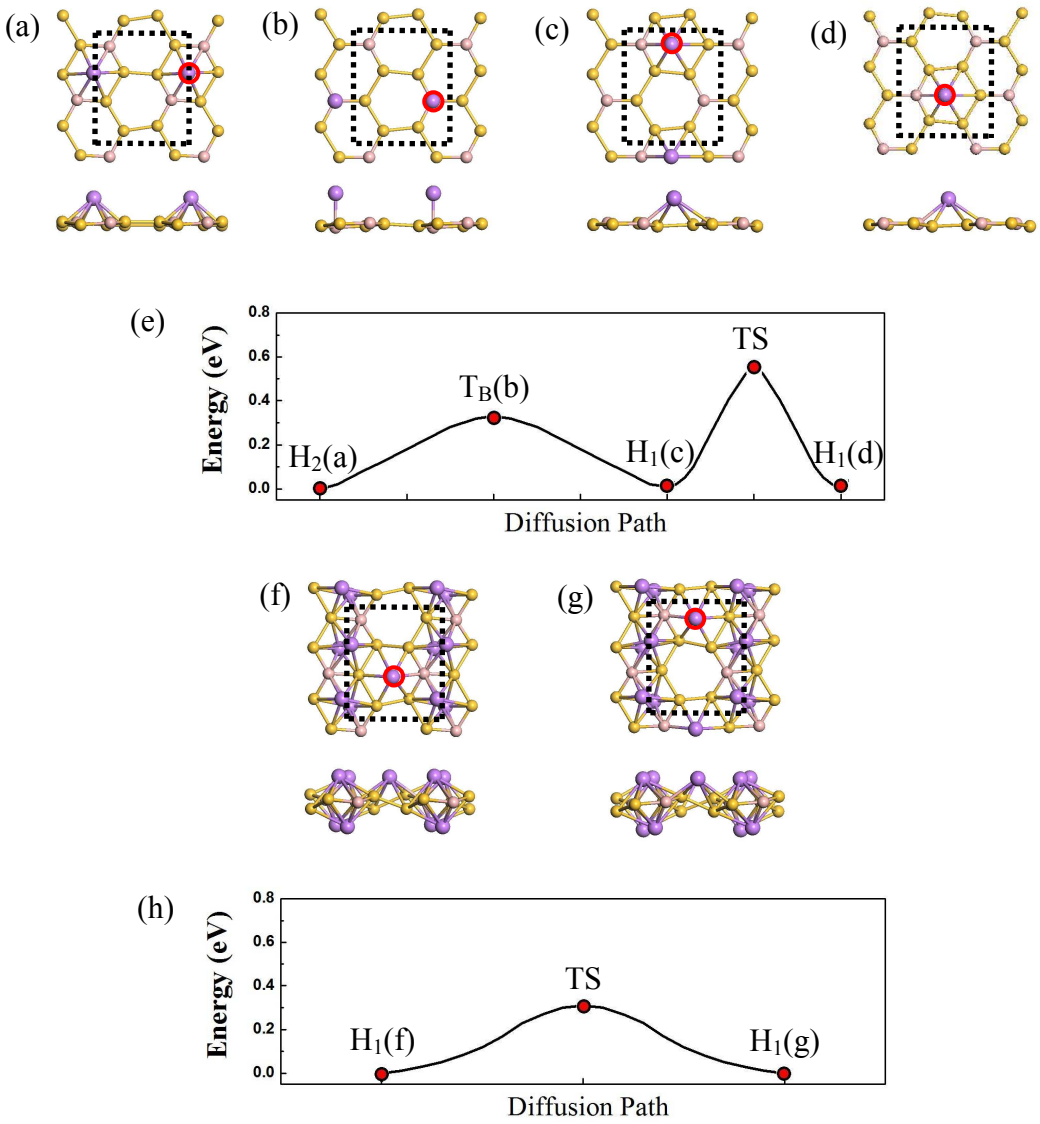

Figure S7. The in-plane diffusion of Li (red circle) on SL *R*-BSi_3 at low Li content (SL-*R*-$Li_{0.11}B_{0.22}Si_{0.67}$, (a) H_2→(b) T_B→(c) H_1→(d) H_1 sites) and at high Li content (SL-*R*-$Li_{0.38}B_{0.15}Si_{0.46}$, (f) H_1→(g) H_1 sites), and the corresponding diffusion pathways and barriers at (e) low and (h) high Li contents, respectively.

To explore the Li diffusion on the SL *R*-BSi_3 (Figure S6), we chose the lithium contents of 0.11 and 0.38 as representatives for the low and high lithiation. Both in-plane diffusion and out-plane diffusion were considered.

For the Li in-plane diffusion at low Li content (SL-*R*-$Li_{0.11}B_{0.22}Si_{0.67}$) (Figure S6a-e), the energy barriers for $H_2 \rightarrow T_B \rightarrow H_1$ and $H_1 \rightarrow H_1$ are 0.33 and 0.56 eV, respectively, indicating that the Li can easily diffuse from H_2 to H_1 through T_B site, however, the diffusion from H_1 to the other H_1 is relatively hard. Similar to the case of the SL *H*-BSi_3, the high energy barrier for the diffusion pathway $H_1 \rightarrow H_1$ can be significantly decreased from 0.56 to 0.31 eV at high Li content (SL-*R*-$Li_{0.38}B_{0.15}Si_{0.46}$) (Figure S6f-h).

For the Li out-plane diffusion, the energy barriers are very high (1.33 and 1.79 eV for H_1 and H_2 sites, respectively), indicating that the out-plane diffusions of Li are energetically prohibited under normal conditions.